`

Substrate-embedded dipole nanoantenna arrays: collective optical response

A. V. Dyshlyuk (orcid.org/0000-0001-5804-6579)[a,b]*, N.A. Inogamov (orcid.org/0000-0002-7703-4415)[c,d,e], O.B. Vitrik (orcid.org/0000-0002-5932-550X)[a]

[a] *Institute of Automation and Control Processes, Far Eastern Branch of the Russian Academy of Sciences (IACP FEB RAS), Vladivostok, 690041 Russia*

[b] *Vladivostok State University (VVSU), Vladivostok, 690041 Russia*

[c]*Landau Institute for Theoretical Physics of Russian Academy of Sciences, Moscow, 142432 Russia*

[d]*Joint Institute for High Temperatures of Russian Academy of Sciences, Moscow, 125412 Russia*

[e]*The Federal State Unitary Enterprise Dukhov Automatics Research Institute, Rosatom, Moscow, 127055 Russia*

**e-mail: anton_dys@iacp.dvo.ru*

Received
Revised
Accepted

Abstract — The paper studies optical properties of a regular array of plasmonic nanoantennas in the form of subwavelength metal spherical particles partly embedded in a metal substrate with a hollow gap between the particles and the substrate. Using gold, a representative plasmonic material, for the particles and the substrate, we have demonstrated that the nanoantenna array possesses two distinct resonances, which may be tuned by varying the parameters of the individual nanoantennas and the grating period. Particluar attention is given to the scenario when the two resonances overlap producing an asymmetric Fano-like resonant feature in the array's reflection spectrum. The possibility of using the nanoantenna array under study for refractometric measurements is considered. Apart from refractometry, the results obtained in this work can find application in the development of novel nanophotonic functional elements for concentration, enhancement and redistribution of the electromagnetic field.

Keywords: Mie scattering, scatterer on substrate, coupled scatterers, metasurface, arrays of nanoantennas, dipole resonance, spherical nanoantenna, plasmonics, nanooptics.

INTRODUCTION

Metamaterials and their two-dimensional analogs, metasurfaces, which possess artificially engineered properties, represent a promising direction in the development of modern optics and photonics [1-8]. Unlike traditional optics, which relies on conventional optical materials with fixed

`

and immutable properties, metamaterials use arrays of nanostructured elements (meta-atoms) to control the phase, amplitude, and polarization of light on a subwavelength scale. This opens up unprecedented possibilities for manipulating and engineering macroscopic optical properties of the resulting material [1-5].

The fundamental structural element of a vast number of metasurfaces [6-8] as well as many other functional photonic structures [9-11], such as bio- and chemosensors [12-15] and surface enhanced Raman scattering platforms [15-19], is a subwavelength plasmonic resonant particle placed on a substrate. Consequently, the light-particle-substrate interaction problem is of major scientific and engineering interest [20-37].

From a theoretical perspective, solving this problem is challenging because the substrate breaks the system's symmetry, even for regularly shaped particles. Furthermore, the outcome is highly dependent on the particle's exact shape, its orientation relative to the substrate, and the substrate's optical properties. The most basic method, suitable for particles much smaller than the wavelength, is to model the particle as a point dipole. Following seminal work by Sommerfeld [21] on a vertical dipole above a flat, lossy surface, many researchers have explored dipole radiation in a half-space.

However, this dipole approximation is only valid under specific conditions: the electromagnetic field must be sufficiently uniform across the particle interior, i.e. retardation effects must be negligible, and the particle must not be too close to the substrate. As the particle nears and touches the substrate, the dipole approximation fails because the particle-substrate coupling causes higher-order multipole contributions to become significant [20].

Researchers have also widely studied light scattering by realistic small particles by explicitly considering their finite size and shape, primarily focusing on regular geometries such as spheres, cylinders, and spheroids. For example, some studies tackle the problem of light scattering by a sphere above a perfectly reflecting mirror [25], while others used Fresnel formulas to handle non-perfectly reflecting substrates [26, 27]. It was also shown that, under certain circumstances the light-scattering problem of a sphere over a substrate can be conceptually divided into two parts: Mie scattering in a uniform medium, plus the reflection of spherical waves off the substrate [28, 29].

A significant body of work on light scattering by particles on substrates utilizes exact integral equations derived from Maxwell's equations with appropriate boundary conditions, which are then solved via standard numerical methods. In this procedure frequent use is made of the extinction theorem from physical optics [30]. Although initially used for analyzing scattering from rough, irregular surfaces, many authors adapted this theorem to calculate both the near and far electromagnetic fields resulting from light scattering by small metallic particles on conducting substrates. The advantage of this approach is that it naturally accounts for multiple interactions between the particle and the substrate [31, 32]. Using this method, researchers have been able to investigate how particle size, distance to the substrate, and the substrate's optical characteristics affect the scattering behavior [33, 34], including the possibility of exciting surface plasmon-polariton waves on conducting surfaces [35-37].

Overall, it should be noted that despite the large volume of publications on light scattering by particles on substrates, most studies assume that the particle is located either directly on or in close proximity to the substrate. The scenario where a plasmonic particle is partially or completely embedded in a substrate with a hollow gap between the particle and the substrate material has not

`

received sufficient attention, even though this configuration presents considerable practical interest. For instance, the authors of [38] studied a disordered 2D array of spherical nickel particles, fabricated via magnetron sputtering in argon atmosphere, embedded with a hollow gap into an optically thick nickel film on a glass substrate. The work demonstrated that the enhanced near field of the nanoantenna in the gap region led to an overall increase in the nickel film's transmittance by more than 25 times compared to a smooth film. This enhancement allowed the authors to observe through the optically thick film the Brillouin oscillations caused by interference of light waves reflected from the film and from the acoustic waves propagating into the substrate, after irradiation of the film with intense femtosecond laser pulses.

In [39] a numerical investigation was carried out into the optical properties of a spherical nickel dipole nanoantenna (NA) embedded in a nickel substrate. However, this work focused exclusively on nickel and did not consider the case of NA and substrate made of noble metals, which are much more popular plasmonic materials. Furthermore, it did not explore the collective optical response of substrate-embedded NA arrays, which is of primary interest for the creation of metasurfaces with properties tailored to specific practical applications. This collective response can be substantially different from that of individual NAs due to their mutual coupling, as well as the appearance of collective modes characteristic of an ordered regular array.

Therefore, the objective of the present work is to investigate the optical properties of regular arrays of noble metal substrate-embedded spherical dipole nanoantennas with due account of both the geometric parameters of individual nanoantennas and the array configuration.

METHODOLOGY OF THE STUDY

The geometry of the plasmonic nanoantenna array under study is shown schematically in Fig.1 (side view in the plane of $\boldsymbol{E}$ and $\boldsymbol{k}$ vector of the incident wave). For the sake of simplicity and clarity, we shall consider in this work a 2D geometry infinitely extended in the z-axis direction before tackling a more general and complicated 3D case in a subsequent study. Furthermore, we shall assume the NAs are embedded into an optically thick metal substrate (effectively a half-space) rather than a thin film, thereby excluding any additional effects associated with the film's backside and transmission of light through it. Therefore, to explore the optical response of the NA array under study we shall use exclusively its reflection spectra upon irradiation of the array with a normally incident plane wave of unit amplitude polarized in the OXY plane. For the material of the particle and substrate we chose gold, which is a typical plasmonic metal. The data on the complex permittivity of gold are taken from reference [40].

Given that an exact analytic solution to the electrodynamic problem of light scattering by the substrate-buried NA array is intractable, we resort to numerical simulation using the Finite-Difference Time-Domain (FDTD) method. To resolve adequately the rounded surface of the nanoantenna, local refinement of the computational grid is applied to the NA region. We use a resolution of 0.3 nm for the refined grid as it was found, during grid convergence study, to be sufficient for the numerical results to be virtually independent of the grid parameters. The size of the computational domain is also chosen so as to ensure that it has no appreciable effect on the simulation results. To model an infinitely extended NA array we use periodic boundary conditions across the y-axis. In the longitudinal direction (across the x-axis) the computational domain is truncated on the left with an

`

absorbing boundary condition in the form of perfectly matched layers (PMLs), while on the right-hand side, the electromagnetic field rapidly decays to zero inside the substrate, rendering the specific type of boundary condition there irrelevant.

RESULTS AND DISCUSSION

To gain insight into the performance of the substrate-buried NA array let us examine its reflection spectrum presented in Fig.2, which was calculated for the array with a period of T=700 nm and three different values of the NAs radius r.

As seen from the figure, the array possesses two distinct resonances. The first one, a narrow high-Q resonance, occurs at the wavelength coinciding with the period of the array and is, therefore, associated with the resonant excitation of the diffraction grating-like electromagnetic mode of the array. Apart from the slight variation in amplitude, it is unaffected by the variation of the NAs radius. The second resonance, centered around λ~1000 nm, exhibits a much wider bandwidth and can be tuned by varying radius R at a rate of approximately 200 nm per 10 nm change in R. This resonance is therefore associated with the optical response of the individual nanoantennas in the array, which, as sown in [39], does indeed experience a red shift of this order of magnitude with an increase in R.

To further validate this proposition, we plot in Figs. 3 and 4 the reflection spectra of the NA array, which were calculated with varying parameters of individual NA while keeping the period of the array fixed. Figure 3 presents the reflection spectra for three different burial depths of the NAs, whereas Figure 4 displays the spectra for three different widths of the gap between the NAs and substrate material. All other parameters are held constant in both figures.

Both figures compellingly demonstrate that changing parameters of the individual NAs affects primarily the second, broadband resonance, hereinafter referred to as the NA resonance (NAR), which red-shifts with increasing NA burial depth and decreasing gap width, in full agreement with the results presented in [39]. The narrowband resonance remains virtually unaffected by the parameters of the individual NAs and can therefore be indeed attributed to the collective response of the array as a periodic structure. We will hereinafter refer to it as the array resonance (AR).

The main parameter defining the position of the array resonance is, naturally, the period of the array T. This is illustrated in Fig. 5, showing the calculated reflection spectra of the NA array for various values of T. The figure is split into two panels to clearly demonstrate the two possible scenarios: the two resonances are separated (Fig. 5a) and they overlap (Fig. 5b).

Fig. 5a shows that, firstly, the array resonance does indeed consistently occur at the wavelength equal to the period of the NA array and, secondly, its amplitude gradually diminishes as it approaches the NA resonance. The latter tendency can be explained by the coupling or hybridization of the ‘collective mode’ of the NA array, which is responsible for AR, and the ‘individual NA mode’ of the array bringing about NAR. The result of this hybridization is most clearly observed in Fig. 5b. As one can see, when AR and NAR overlap, the shape of the spectral response of the array is dramatically modified and distorted. The appearance of the asymmetric Fano line shape is evident, which is a well-known signature of coupling between narrowband and broadband resonant states.

The line shape resulting from AR and NAR overlap can be manipulated and fine-tuned by simultaneously adjusting several parameters of the individual nanoantennas. This must be done so that the resultant NAR shifts largely cancel each other and its wavelength remains approximately

`

unchanged, thus keeping the resonances overlapped. To illustrate this point we show in Fig. 6 the overlapped resonance line shape for three distinct combinations of the gap width and NA burial depth.

As evident from the plots, with these combinations of parameters one can obtain at a fixed wavelength in the reflection spectrum either a shallow sine-like feature or more and less sharp and deep slightly asymmetric Fano line shapes. This opens up exciting prospects of tailoring the collective spectral response of the NA array to specific practical applications.

Another effect that is introduced by arranging substrate-buried nanoantennas in a regular array is the radiative coupling between the individual NAs, which can significantly modify the reflection spectrum of the array when the individual NAs are very close together. This effect is not observed at the array periods of Figs. 5-6 and appears at much smaller values of T, for which AR is no longer significant as it is blue-shifted far into the ultraviolet range. To illustrate this effect, Fig 7. shows the calculated reflection spectra of the NA array for T ranging from 500 nm (no radiative coupling) to 110 nm (very strong radiative coupling).

As seen from the figure, the radiative coupling between individual NAs brings about gradual smearing and broadening of NAR and it becomes almost washed-out at T=110 nm.

Finally, in view of potential refractometric applications of the NA array under study, let us consider the effect of the ambient refractive index on its reflection spectrum, as shown in Fig. 8.

As seen from the presented results, the refractive index of the ambient medium has a pronounced effect on the positions of both resonances. However, the refractometric sensitivity of the array resonance (which shifts in direct proportion to n_0) turns out to be about 3 times higher than that of NAR (AR: 680 nm per refractive index unit (RIU), NAR: 220 nm/RIU). This causes the two resonances, which were initially separated (at n_0~1), to gradually approach each other and merge together as they both are red-shifting with increasing n_0.

CONCLUSIONS

Thus, in this work we have studied the collective optical response of an infinite array of substrate-buried plasmonic dipole nanoantennas in the form of subwavelength spherical gold particles embedded in the gold substrate with a hollow gap between the particle and the substrate material. To maximize clarity of the demonstration of the array's optical properties we adopted a 2D geometry consisting of a 1D array of infinitely long cylindrical wires of circular cross-section embedded in an optically thick substrate.

It was shown that the substrate-embedded NA array posses two distinct resonances. One of them is a high-Q narrowband resonance associated with the collective response of the array as a diffraction grating and it occurs at the wavelength equal to the array's period. The second, broadband resonance is associated with the optical response of the individual nanoantennas and can be tuned in a wide spectral range by varying NAs' parameters such as their radius, gap width and burial depth. Depending on these parameters and the array's period, the two resonances may either overlap or be separated. In the former case an asymmetric resonant feature was shown to appear in the array's reflection spectrum, often with a characteristic Fano-like profile. It was demonstrated that the exact resulting line shape can be manipulated and fine-tuned by simultaneously varying several parameters of the individual NAs so that the two resonances keep overlapping. This opens up exciting prospects of tailoring the collective spectral response of the NA array to specific practical applications.

`

It was also demonstrated that the mutual radiative coupling between NA, which occurs in an array with a small period when the individual NAs are very close together, leads the smearing and broadening of the NA resonance and it becomes almost washed-out at T=110 nm.

Finaly, we showed that both resonances possess notable sensitivity to the refractive index of the ambient dielectric medium, which enables the use of the substrate-embedded NA array for carrying out precise refractometric measurements. The sensitivity of the array resonance (680 nm/RIU) was demonstrated to be about 3 times higher than that of the nanonantenna resonance (220 nm/RIU).

Apart from possible application in refractometry, the results obtained in the work can find application in plasmonics, nanooptics and nanophotonics for designing novel functional elements to concentrate, enhance or redistribute electromagnetic field.

FUNDING

The presented study is performed within the state task of IACP FEB RAS (121021600267-6, FWFW-2021-0001).

CONFLICT OF INTEREST

The authors declare that they have no conflicts of interest.

`

REFERENCES

1. Zheludev, N. I., & Kivshar, Y. S. *Nature materials*, 2012, vol. 11, no 11, p. 917-924.
2. Cui, T. J., Smith, D. R., & Liu, R. *Metamaterials* (p. 1). New York: Springer, 2010.
3. Liu, Y., & Zhang, X. *Chemical Society Reviews*, 2011, vol. 40, no 5, p. 2494-2507.
4. Kshetrimayum, R. S. *IEEE potentials*, 2004, vol. *23, no* 5, p. 44-46.
5. Valipour, A., Kargozarfard, M. H., Rakhshi, M., Yaghootian, A., & Sedighi, H. M. *Proceedings of the Institution of Mechanical Engineers, Part L: Journal of Materials: Design and Applications*, 2022, vol. 236, no. 11, p. 2171-2210.
6. Zhang, G., Lan, C., Bian, H., Gao, R., & Zhou, J., *Optics Express*, 2017, vol. *25,* no. 18, p. 22038.
7. Holloway, C. L., Kuester, E. F., Gordon, J. A., O'Hara, J., Booth, J., & Smith, D. R., *IEEE antennas and propagation magazine*, 2012, vol. *54,* no. 2, p. 10.
8. Alvarez-Fernandez, A., Cummins, C., Saba, M., Steiner, U., Fleury, G., Ponsinet, V., & Guldin, S., *Advanced Optical Materials*, 2021, vol. *9,* no. 16, p. 2100175.
9. Tonkaev, P., & Kivshar, Y., *JETP Letters*, 2020, vol. 112, no. 10, p. 615.
10. Berestennikov, A., Pushkarev, A. P., & Makarov, S. V., *Bulletin of the Russian Academy of Sciences: Physics*, vol. 86, Suppl. no. 1, p. 20.
11. Melnik, N. N., Sherstnev, I. A., & Tregulov, V. V. *Bulletin of the Russian Academy of Sciences: Physics*, 2021, vol. 85, p. 990.
12. Aristov, A. I., Zywietz, U., Evlyukhin, A. B., Reinhardt, C., Chichkov, B. N., & Kabashin, A. V., *Applied Physics Letters*, 2014, vol. 104, no. 7.
13. Kuznetsov, A. I., Evlyukhin, A. B., Gonçalves, M. R., Reinhardt, C., Koroleva, A., Arnedillo, M. L., ... & Chichkov, B. N., *ACS nano*, 2011, vol. 5, no. 6, p. 4843.
14. Su, X., Gao, L., Zhou, F., & Duan, G., *Sensors and Actuators B: Chemical*, 2017, vol. *251*, p. 74.
15. Yockell-Lelièvre, H., Lussier, F., & Masson, J. F., *The Journal of Physical Chemistry C*, 2015, vol. *119, no.* 51, p. 28577.
16. Wu, J., Yang, X., & Fang, J., *Particle & Particle Systems Characterization*, 2019, vol. *36, no.* 8, p. 1900268.
17. Christie, D., Lombardi, J., & Kretzschmar, I., *The Journal of Physical Chemistry C*, 2014, vol. *118, no.* 17, p. 9114.
18. Zhang, H., Zhou, F., Liu, M., Liu, D., Men, D., Cai, W., ... & Li, Y., *Advanced Materials Interfaces*, 2015, vol. *2, no.* 9, p. 1500031.
19. Kukushkin, V. I., Astrakhantseva, A. S., & Morozova, E. N. *Bulletin of the Russian Academy of Sciences: Physics*, 2021, vol. 85, p. 133.
20. Moreno, F., Saiz, J. M., & González, F., Light Scattering by Particles on Substrates. Theory and Experiments, chapter in *Light scattering and nanoscale surface roughness*, 2007, p. 305-340.
21. A. Sommerfeld, Partial differential equations in physics, New York, Academic Press, 1967.
22. Chew, W.C. Waves and fields in inhomogeneous media., Van Nostrand Reinhold, 1990.
23. Felsen, L. B., & Marcuvitz, N. Radiation and scattering of waves, vol. 31, John Wiley & Sons, 1994.
24. Novotny, L.: Principles of nano optics, Cambridge University Press., 2006.
25. Nahm, K. B., & Wolfe, W. L., *Applied optics*, 1987, vol. 26, no. 15, p. 2995.
26. Weber, D. C., & Hirleman, E. D. *Applied optics*, 1988, vol. *27, no.* 19, p. 4019.
27. Moreno, F., Saiz, J. M., Valle, P. J., & González, F., *Applied physics letters*, 1996, vol. *68,* no. 22, p. 3087.
28. Bobbert, P. A., & Vlieger, J., *Physica A: Statistical Mechanics and its Applications*, 1986, vol. 137, no. 1-2, p. 209.

`

29. Bobbert, P. A., Vlieger, J., & Greef, R. *Physica A: Statistical Mechanics and its Applications*, 1986, vol. *137, no.* 1-2, p. 243.
30. Vesperinas, M. N. Scattering and diffraction in physical optics., World Scientific Publishing Company, 2006.
31. Valle, P. J., González, F., & Moreno, F., *Applied optics*, 1994, vol. 33, no. 3, p. 512.
32. Valle, P. J., Moreno, F., Saiz, J. M., & González, F., *Physical Review B*, 1995, vol. *51, no.* 19, p. 13681.
33. Saiz, J. M., Valle, P. J., González, F., Ortiz, E. M., & Moreno, F., *Optics letters*, 1996, vol. 21, no. 17, p. 1330.
34. Valle, P. J., Moreno, F., Saiz, J. M., & Gonzalez, F. *IEEE Transactions on Antennas and Propagation*, 1996, vol. *44, no.* 3, p. 321.
35. Valle, P. J., Moreno, F., & Saiz, J. M., *JOSA A*, 1998, vol. *15, no.* 1, p. 158.
36. Dyshlyuk, A. V., Proskurin, A., Bogdanov, A. A., & Vitrik, O. B., *Nanomaterials*, 2021, vol. 11, no. 11, p. 2937.
37. Dyshlyuk, A. V., Bogdanov, A. A., & Vitirk, O. B., *Computer Optics*, 2020, vol. *44, no.* 6, p. 893.
38. Petrov Y.V., Romashevskiy S.A., Dyshlyuk A.V., Khokhlov V.A., Eganova E.M., Polyakov M.V., Evlashin S.A., Ashitkov S.I., Vitrik O.B., Inogamov N.A. JETP, 2025, vol. 167, no 5, p. 645-671.
39. Dyshlyuk, A. V., Inogamov, N. A., & Vitrik, O. B. *Bulletin of the Russian Academy of Sciences: Physics*, 2024, vol. *88*(Suppl 3), p S450-S456.
40. Johnson, P. B., & Christy, R. W. *Physical review B*, 1972, vol. *6, no.* 12, p. 4370.

`

FIGURE CAPTIONS

Fig. 1 Schematic drawing of the unit cell of the NA array and its parameters (1 – dielectric medium with refractive index n_0, 2 – gold with dielectric permittivity ε_{Au}).

Fig. 2 Calculated reflectivity spectra of the NA array for three values of the NA radius: *r*=45, 50 and 55 nm. Other parameters are as follows: n_0=1, *d*=5 nm, *h*=25 nm, *T*=700 nm.

Fig. 3 Calculated reflectivity spectra of the NA array for three values of the NA burial depth: *h*=15, 25 and 35 nm. Other parameters are as follows: n_0=1, *d*=5 nm, *r*=50 nm, *T*=700 nm.

Fig.4 Calculated reflectivity spectra of the NA array for three widths of the gap between the NA and substrate material: d=4, 5 and 6 nm. Other parameters are as follows: n_0=1, h=25 nm, *r*=50 nm, *T*=700 nm.

Fig. 5 Calculated reflectivity spectra of the NA array for various periods of the array. Illustrated in the two panels are the cases when the array resonance and the nanoantenna resonances do not (Fig 5a, T=600, 700 and 800 nm) and do (Fig 5b, T=900, 1000, 1100 and 1200 nm) overlap. Other parameters are as follows: n_0=1, h=25 nm, *r*=50 nm, d=5nm.

Fig. 6 Calculated reflectivity spectra of the NA array for three combinations of the gap width between the NA and substrate material and NA burial depth: d=2nm, h=44 nm; d=8.5 nm, h=32 nm; d=15 nm, h=20 nm. The combinations are chosen so as to keep the AR and NAR overlapped. Other parameters are as follows: n_0=1, *r*=50 nm, *T*=900 nm.

Fig. 7 Calculated reflectivity spectra of the NA array for various (small) periods of the array T=110, 200, 300 and 500 nm. Other parameters are as follows: n_0=1, h=25 nm, *r*=50 nm, d=5nm.

Fig. 8 Calculated reflectivity spectra of the NA array for various values of the refractive index of the ambient dielectric medium: n_0=1, 1.1, 1.2, 1.3, 1.4 and 1.5. Other parameters are as follows: h=25 nm, *r*=50 nm, d=5nm, T=700 nm.

`

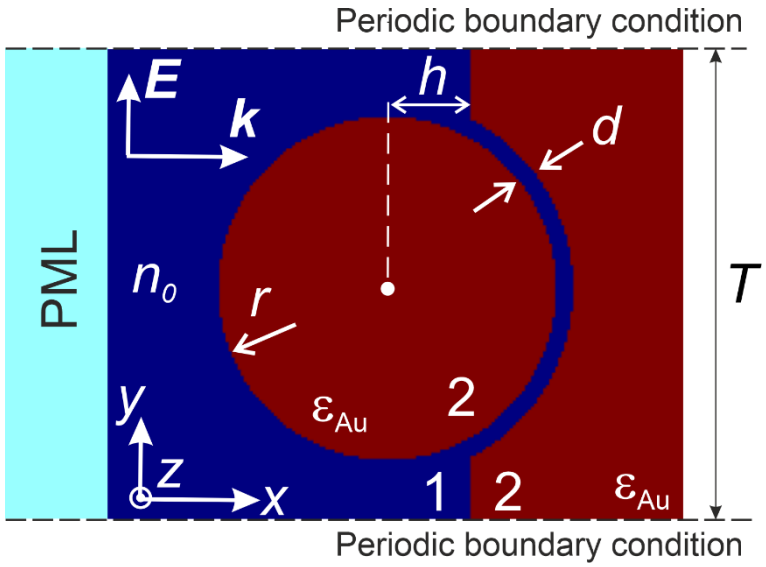
Periodic boundary condition
E
k
h
d
PML
n_0
r
T
y
z
x
ε_{Au}
2
1
2
ε_{Au}
Periodic boundary condition

Fig. 1

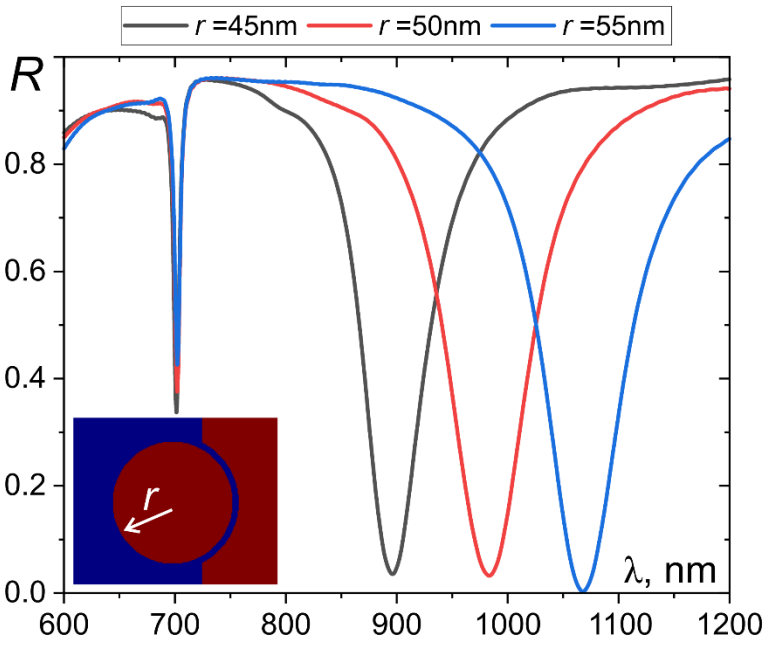
r =45nm
r =50nm
r =55nm
R
0.8
0.6
0.4
0.2
0.0
r
λ, nm
600
700
800
900
1000
1100
1200

Fig. 2

`

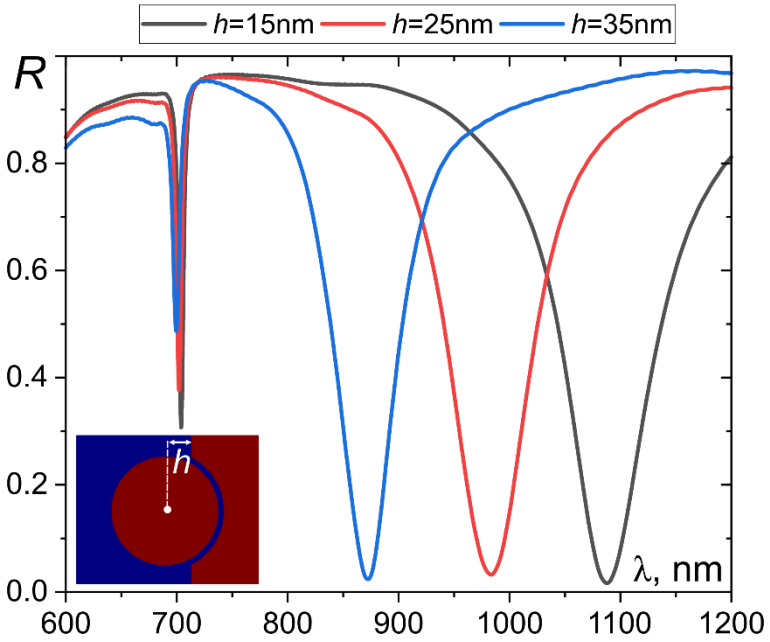
h=15nm
h=25nm
h=35nm
R
0.8
0.6
0.4
0.2
0.0
h
λ, nm
600
700
800
900
1000
1100
1200

Fig.3

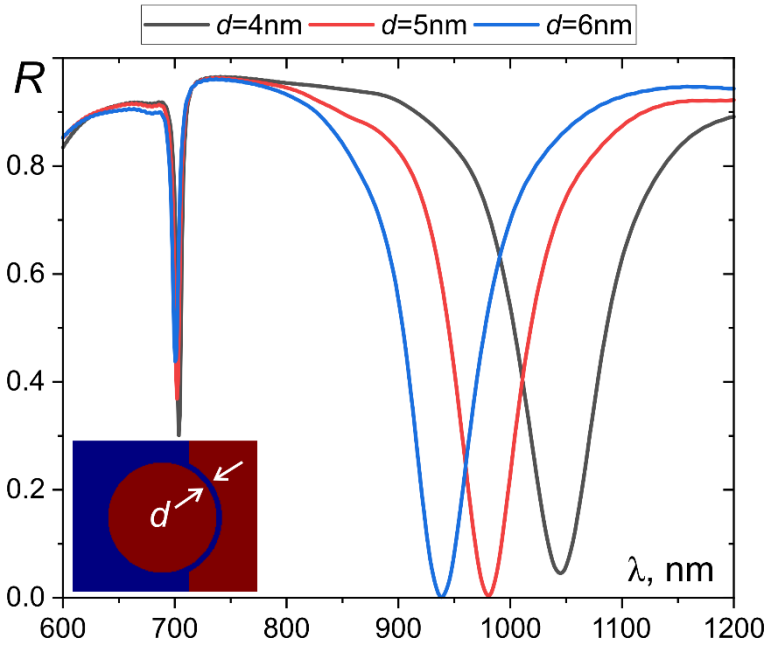
d=4nm
d=5nm
d=6nm
R
0.8
0.6
0.4
0.2
0.0
d
λ, nm
600
700
800
900
1000
1100
1200

Fig. 4

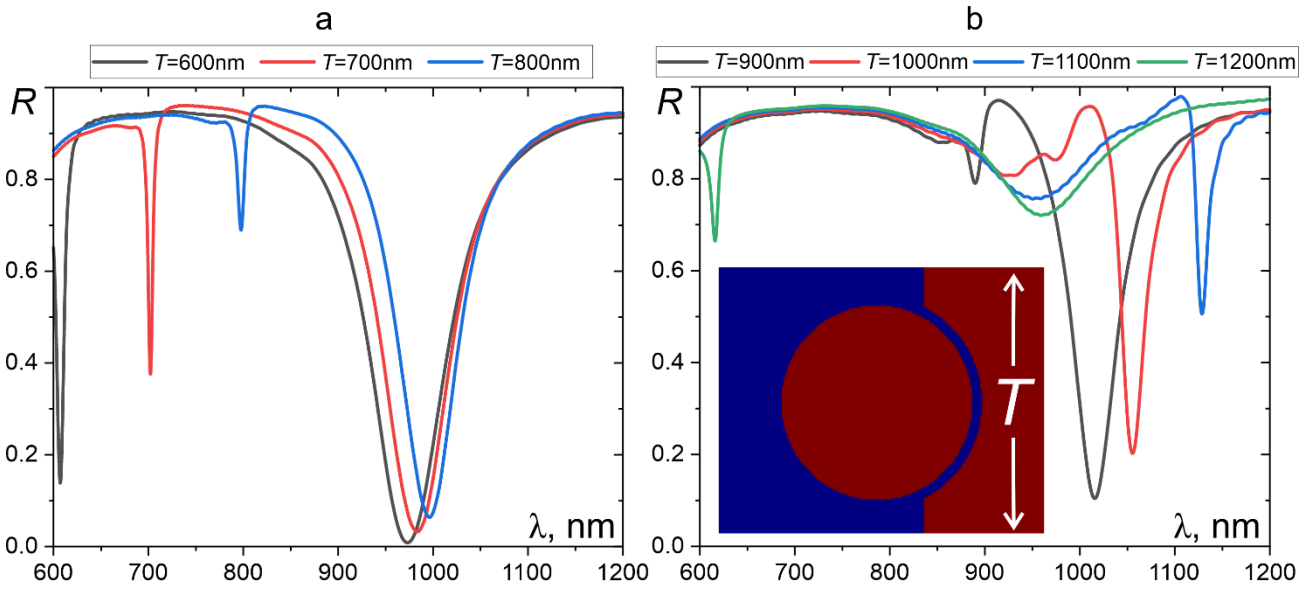
a
b
T=600nm
T=700nm
T=800nm
T=900nm
T=1000nm
T=1100nm
T=1200nm
R
λ, nm
T

Fig. 5

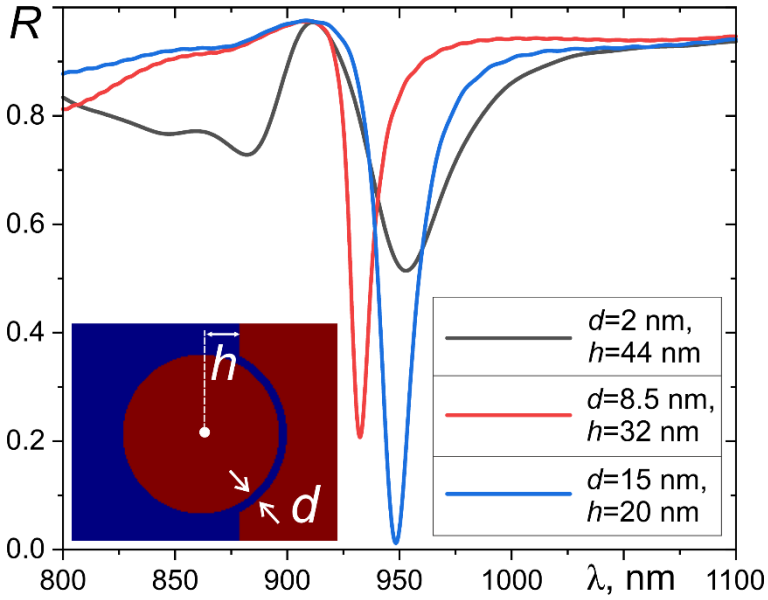
R
λ, nm
h
d
d=2 nm,
h=44 nm
d=8.5 nm,
h=32 nm
d=15 nm,
h=20 nm

Fig.6

`

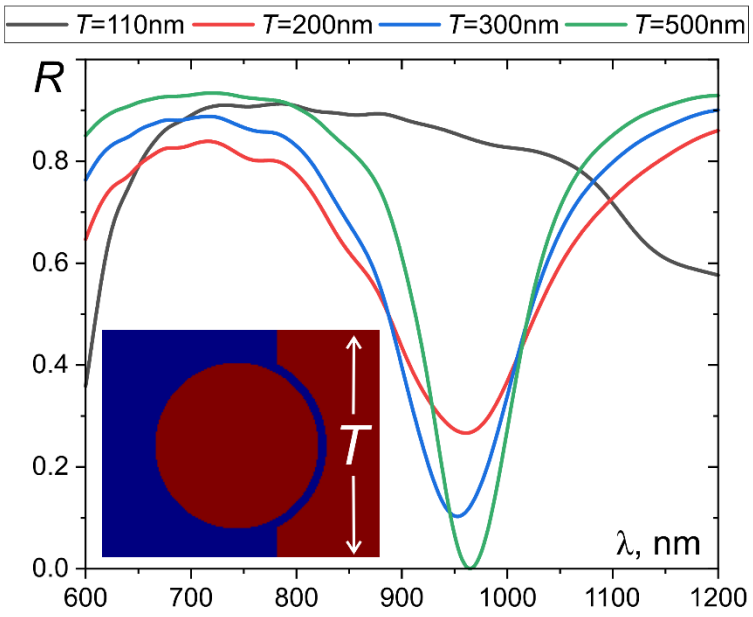
T=110nm
T=200nm
T=300nm
T=500nm
R
0.0
0.2
0.4
0.6
0.8
600
700
800
900
1000
1100
1200
λ, nm
T

Fig. 7

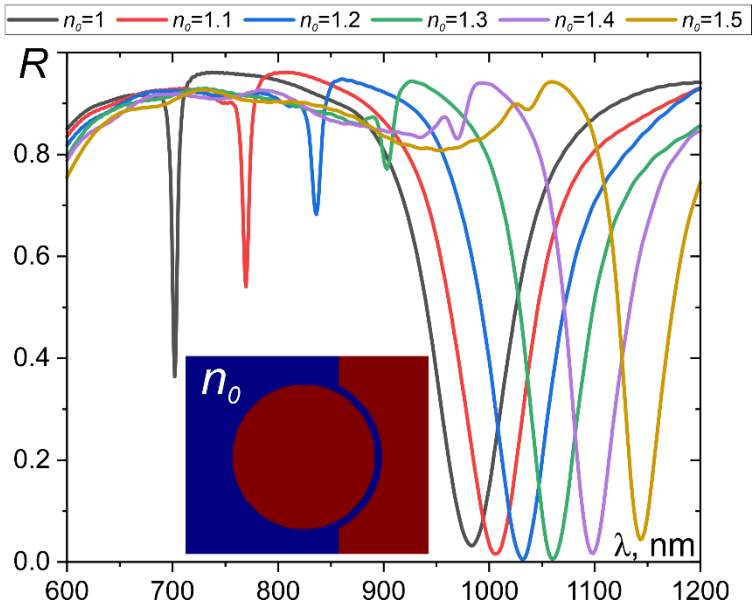
n0=1
n0=1.1
n0=1.2
n0=1.3
n0=1.4
n0=1.5
R
0.0
0.2
0.4
0.6
0.8
600
700
800
900
1000
1100
1200
λ, nm
n0

Fig. 8